Nonlocal response in CdTe photovoltaics

Diana Shvydka,[a] A. D. Compaan, and V. G. Karpov
Department of Physics and Astronomy, University of Toledo, Toledo, Ohio 43606

(Received 13 February 2002; accepted for publication 6 March 2002)

We have studied the nonlocal photovoltaic response to a laser beam in CdTe/CdS solar cells. The laser-generated plasma is shown to spatially decay over a considerable distance that depends on the device lateral resistance and laser beam power. This affects open circuit voltage far from the laser spot. For the case when the lateral resistance is dominated by the transparent conductive oxide (in completed devices), it is shown that the characteristic decay length may be as long as 1 m. For the alternative case of unfinished devices that do not have a metal layer, the semiconductor layer sheet resistance dominates the nonequilibrium plasma spreading, and the characteristic decay length falls into the range of tenths of a millimeter. Also associated with such nonlocal response are features in photoluminescence mapping, where different excitation powers lead to different map topologies. We have developed a theory that expresses the effects of laser-generated plasma spreading in terms of the semiconductor film photovoltaic parameters. © *2002 American Institute of Physics.*
[DOI: 10.1063/1.1473696]

I. INTRODUCTION

In many applications nonequilibrium electrons and holes in a *p-n* junction are created nonuniformly in the lateral direction. One example is the laser-generated electron–hole plasma. Charge carrier generation by a uniform light in laterally nonuniform photovoltaics exhibits another such example.

It is typically assumed in the above applications that the nonequilibrium carriers do not propagate far from their birthplace. This hypothesis of locality has numerous implications. In particular, it underlies photoluminescence (PL),[1] micro-PL,[2] electron beam induced current,[3,4] and optical beam induced current[5,6] mapping techniques of studying material local properties. According to the hypothesis, the charge carrier lateral diffusion is relatively inefficient, i.e., the nonequilibrium carriers recombine before traveling distances comparable to the nonuniformity scale.

Indeed, estimates for different photovoltaics indicate the diffusion lengths in the range of one to several microns, much shorter than the typical laser beam diameter. It should be remembered however that such estimates depend on the bias conditions and are typically obtained from the measurements under the light. If, to the contrary, we consider the diffusion length beyond the light exposed area, its value can be considerably larger for the following two reasons. First, due to lateral spreading, the carrier concentration falls off and therefore their recombination slows down; hence the charge carriers survive longer. Second, because of the concentration falloff, the electric field generated by the nonequilibrium carriers weakens and thus opposes less the original built-in field that separates the carriers and slows down the recombination.

The above reasoning can be equally worded in the terms of an equivalent circuit representing a large area *p-n* junction, which is a set of many diodes connected in parallel through lateral resistors, with the second connector being a metal bus whose resistance can be neglected (Fig. 1). An electric current source in parallel with the diodes mimics the local electron–hole generation by light. As an alternative one can consider the current source of the opposite sign that mimics a shunt through or the device physical edge where the electron–hole recombination is more efficient. The lateral current flows through the resistors and branches out to the conductive bus, the latter process representing electron–hole recombination. This kind of branching is similar to the well-known process that determines the voltage decay in a transmission line, the latter being represented by the circuit in Fig. 1 with resistors instead of diodes. Because of the branching, the local electric potential in the circuit decays with the distance from the current source. An important feature is that, because the diode current depends on electric potential exponentially, the branching here will become much less significant than it would be for the case of the standard transmission line. Hence, long range lateral spreading becomes possible. Indeed, we shall see in what follows that the electric potential in the circuit decays with the distance logarithmically, rather than exponentially, as it would take place for the standard transmission line.[7]

Depending on the device design the lateral resistors can be either conductive contacts to or the semiconductor layers themselves. In the former case the transparent conductive oxide (TCO) is the typical higher resistivity contact. Its sheet resistance is much lower than that of the semiconductor and it does not have noticeable bias dependence. On the contrary, the lateral resistance is strongly bias-dependent when a semiconductor dominates it. With the above in mind we will discriminate between the two implementations of the circuit of Fig. 1: (i) bias-independent low lateral resistance dominated by TCO, and (ii) bias-dependent high lateral resistance dominated by the more conductive of the two semiconductor junction layers.

[a]Electronic mail: dshvydka@physics.utoledo.edu

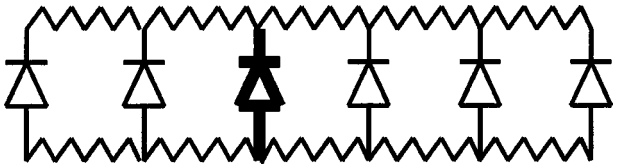

FIG. 1. Equivalent circuit representing the electric current spatial decay. Bold piece stands for the current source corresponding to the laser excitation.

In this paper we present observations of nonlocal optical response in CdTe photovoltaics for both of the above implementations. Our data show, indeed, very significant electron–hole plasma spreading. For the case of TCO-dominated resistivity, the spreading goes over dozens of centimeters, exceeding practical device sizes. This case provides simple settings for verifying the physics of the phenomenon when the lateral sheet resistance is uniform and bias independent. For the case of semiconductor-dominated lateral spreading our data are indicative of unexpectedly low and nonuniform semiconductor sheet resistance. This finding is verified by the data on PL mapping. Also, we present a theory that describes the observed spreading quantitatively and we discuss its possible other implications.

II. THEORY

As long as we attribute the observed phenomena to the plasma lateral spreading in the device, the related theoretical problem becomes that of the steady-state spatial electric potential distribution generated by the laser beam striking a *p-n* junction of a given dimensionality. We describe the system as a set of microdiodes in parallel, in which a certain local region mimics the area under the beam and is different from the rest of the system; the equivalent circuit is shown in Fig. 1. The diode interconnects are responsible for the lateral resistance and are characterized by their specific resistances (per length or per area in one dimensional (1D) or 2D geometry, respectively). As discussed earlier, depending on the experimental design, the effective lateral resistance may be due to either the TCO (when the metal back contact is present) or, alternatively, to a semiconductor layer. In what follows we analyze separately the cases of different geometries.

A. 1D, infinite sample

For the 1D case, the photovoltaic I/V equation and Ohm's law describe the electric potential distribution in the system depending on the coordinate x:

$$\frac{dJ}{dx}=-j_0\left[\exp\left(\frac{\varphi}{T}\right)-1\right]+j_L, \quad J=-\rho\frac{d\varphi}{dx}. \tag{1}$$

Here J is the lateral current, j_0 and j_L are the thermal and light-induced components of the diode currents per length, respectively, and ρ is the resistance per length. Here we use units for which the Boltzmann's constant and the electron charge are set equal to unity. Also, the temperature in Eq. (1) may include (as a hidden multiplier) the diode nonideality factor, which is known to vary in the range from 1 to approximately 4 in different diode structures.[8] The representation in Eq. (1) equally applies to both the ''dark'' and ''light'' (under the beam) regions. Because the parameters corresponding to those regions are different, so are their local open circuit voltages:

$$V_{\rm oc}=T\ln\left(\frac{j_L}{j_0}+1\right)\neq V'_{\rm oc}=T\ln\left(\frac{j'_L}{J'_0}+1\right). \tag{2}$$

where the primed quantities correspond to the light area. The latter difference results in a local forward bias; hence, an electric field that forces a lateral current J. Because of the distributed resistance ρ, the electric potential and the current decay over some distance L called the screening length.

Equation (1) is known to describe the effects of distributed resistance of TCO.[9] It applies here with a new feature that the resistivity may be bias dependent: $\rho=\rho(\varphi)$. This happens when a semiconductor (rather than the TCO) is responsible for lateral resistance, because the semiconductor resistivity is bias dependent. To derive the dependence $\rho=\rho(\varphi)$ we note that the voltage across the *p-n* junction can be represented as a difference between the quasi-Fermi levels of the electrons and holes, each of the contributions being proportional to the logarithm of the corresponding carrier concentration. Therefore, the charge carrier concentrations depend exponentially on the voltages across the corresponding *p*- and *n*-semiconductor layers. Because, on the other hand, the resistivity is inversely proportional to the carrier concentration, one can write

$$\rho=\rho_0\exp\left(-\frac{\alpha\varphi}{T}\right). \tag{3}$$

Here α (<1) is the fraction of the entire voltage drop corresponding to a given semiconductor layer. Because it is unlikely that the layers have comparable resistances, we will consider one of them, whose lateral resistance is responsible for the plasma spreading (which is assumed to be the *p*-type layer in our experimental design). In the framework of this consideration, α remains a phenomenological parameter. Its value is determined by the characteristics of the *n*- and *p*-layers constituting the device.[10]

We choose the origin ($x=0$) at the beam center, the beam edges are at $|x|=d/2$, and the entire setup is symmetric with respect to the origin. Then, associated with Eq. (1) the boundary conditions will be at the beam edge ($x=d/2$) and at infinity,

$$\begin{aligned}&\frac{1}{\rho}\frac{d\varphi}{dx}=J_L, \quad \text{for } x=d/2,\\ &\varphi=V_{\rm oc}, \quad \frac{d\varphi}{dx}=0, \quad \text{for } x=\infty.\end{aligned} \tag{4}$$

Here J_L is the current generated under the beam. The first of the latter conditions imply the case of a narrow beam, $d\ll L'_0$, where L'_0 is the screening length under the laser beam, which corresponds to the experimental conditions in this work. Under such conditions the electric potential under the beam is considerably smaller than $V'_{\rm oc}$ (the nonequilibrium plasma is swept away from the inner beam region). In the

opposite limiting case $d \gg L_0'$, the electric potential under the beam reaches its saturated value V_{oc}' very close to the beam edge, and the boundary condition reduces to $\varphi(d/2) = V_{oc}'$.

Eqs. (1) and (3) with the boundary conditions in Eq. (4) can be solved as is described in the Appendix below. As a result the electric potential distribution in the dark region is given by

$$\varphi = \varphi_0 - \frac{2T}{1-\alpha} \ln\left(1 \pm \frac{x}{L}\right), \quad \text{for } \varphi - V_{oc} \gg T, \tag{5}$$

where the sign must be chosen to give the solution that decays with x: $(+)$ for $\alpha < 1$, $(-)$ for $\alpha > 1$. The electric potential at the laser beam edge,

$$\varphi_0 = V_{oc} + T \frac{2}{1+\alpha} \ln\left[\frac{|1-\alpha|}{2} \sqrt{\frac{1+\alpha}{2\alpha}} \frac{J_L \rho_0 L}{T}\right], \tag{6}$$

where L is the screening length,

$$L = L_0 \left[\left(\frac{\alpha+1}{2\alpha}\right)^{\alpha/\alpha-1} \frac{1-\alpha}{2\alpha} \frac{J_L}{(j_0 + j_L) L_0}\right]^{\alpha - 1/\alpha + 1}, \tag{7}$$

and L_0 is the screening length for the case of a small perturbation, $\varphi - V_{oc} \ll T$,

$$L_0 = \left[\frac{T}{\alpha \rho_0 (j_L + j_0)} \left(\frac{j_L + j_0}{j_0}\right)^{\alpha}\right]^{\frac{1}{2}}. \tag{8}$$

Note that while the above equations may seem inapplicable for $\alpha = 1$, it can be shown[9] that for $\alpha = 1$ the logarithmic coordinate dependence $\varphi(x)$ turns into quadratic one and the screening length L coincides with L_0.

B. 1D, finite sample

Applying the boundary condition at infinity implies a considerable sample size. We shall see in the next section that, for the case of TCO-dominated lateral effects, the screening length becomes much greater than the sample size. Therefore we will need an equation that describes the electric potential decay in a finite size sample. The main change is coming with the boundary condition that the current vanishes at the sample end ($x = \ell$). As is derived in the Appendix, the required equation takes the form

$$\varphi = V_{oc} + T \ln A - 2T \ln\left\{\cos\left[\sqrt{\frac{A}{2}} \left(\frac{\ell - x}{L_0}\right)\right]\right\}. \tag{9}$$

In accordance with the boundary conditions at the laser beam edge [see Eq. (4)], the parameter A is a solution to the transcendental equation

$$\frac{J_L}{j_L L_0} = A\sqrt{2} \tan\left(\frac{\ell}{L_0} \sqrt{\frac{A}{2}}\right). \tag{10}$$

C. 2D case

For the 2D case, Eq. (1) remains formally the same, with j_L and j_0 standing for the currents per area and ρ being the sheet resistance. J becomes a vector, and the derivatives in dJ/dx and $d\varphi/dx$ must be replaced by the operators div and grad, respectively. As it often happens with 2D problems, there is no analytical solution covering the whole range of distances x. It is shown in the Appendix that in the region of $x \gg L$ the solution retains its 1D form of Eq. (5). In the complementary regions of small $x \ll L$ the solution takes the form

$$\varphi = \varphi_1 + \frac{T}{\alpha - 1} \ln\left[1 \pm \left(\frac{x}{L}\right)^2\right], \tag{11}$$

where the screening length

$$L = 2L_0 \exp\left[\frac{(\alpha-1)(V_{oc} - \varphi_1)}{2T}\right]. \tag{12}$$

Here φ_1 is the electric potential in the center of the beam ($x = 0$), which differs from φ_0 in Eq. (6) by a numerical factor (of the order of one). For the purposes of this work Eqs. (11) and (12) have practically no region of applicability, since the 2D geometry is implemented here for the conditions of semiconductor-controlled lateral spreading in which L is relatively short. As a result all the data fall into the range of distances larger than L, which is accurately approximated by the 1D expressions.

Overall, the following qualitative conclusions can be drawn from the above results: (i) the screening length L decreases with the excitation current J_L, in accordance with Eq. (7); (ii) L is independent of the ambient light current as it follows from combining Eqs. (7) and (8); (iii) the amplitude of the laser beam induced electric potential [Eq. (6)] logarithmically increases with the excitation current and does not depend on the ambient light current; (iv) the electric potential perturbation decays logarithmically with the distance from the laser beam; and (v) the low-excitation screening length L_0 [Eq. (8)] decreases with the ambient light intensity.

A comment is in order regarding semiconductor-controlled lateral spreading in polycrystalline and amorphous materials. The above model does not account for possible in-plane nonuniformities in noncrystalline semiconductors and thus can only be valid if the screening length L is larger than the space scale of in-plane nonuniformity. The latter was shown to span up to 1 mm in polycrystalline CdTe,[11] which distance is comparable to or greater than the observed screening length (see the next section). That is why, as opposed to the case of TCO-controlled lateral spreading, the above theory is not expected to give an exact quantitative description of the semiconductor-controlled lateral spreading, and will serve only as a semiquantitative guide.

III. EXPERIMENT

For this study solar cell devices were prepared by the vapor transport deposition (VTD) and radio-frequency magnetron sputtering techniques. A layer of CdS followed by a CdTe layer was deposited on commercially available SnO_2:F-coated glass substrates. The TCO layer (SnO_2:F) served as a front electrode. After deposition, the samples were submitted to a standard anneal in the presence of $CdCl_2$ vapor which generally leads to improved electrical characteristics.[12]

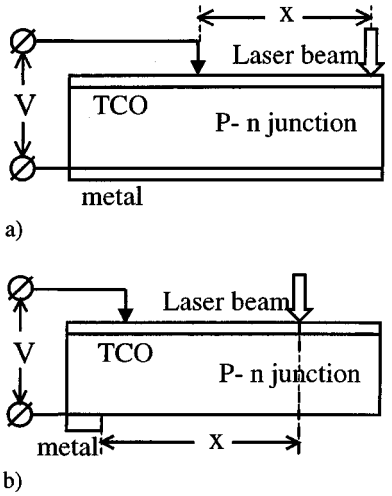

FIG. 2. Side view of the one-dimensional setup for studying voltage vs distance x from the laser beam for the cases when the lateral spreading is dominated by (a) TCO and (b) the semiconductor layer. The total device thickness was in the range 3–4 μm. The drawing does not show a relatively thick (3 mm) glass substrate above the TCO.

For the case of the TCO-dominated lateral spreading, the devices were finished with a metal layer deposited to form the back contact to CdTe [Fig. 2(a)]. Such cells were made one dimensional of width 3 mm and length 20 cm.

For the semiconductor dominated lateral spreading we used the design in Fig. 2(b) in which the open circuit voltage V_{oc} was measured between a dot cell metal contact and the TCO. The dot cell (metal) area was 1.1 cm^2. To make an ohmic contact to the CdTe film without a metal in some experiments we used a commercially available (antistatic) carbon foam of the characteristic resistance of several $k\Omega$. Both 1D and 2D geometries were studied. To keep links between the 2D and 1D cases, the linear cells were scribed out on the basis of the originally roundish 2D dot cells as is shown in Fig. 3. Both mechanically and laser scribed 1D cells were made.

The photovoltage was generated with a 752 nm line of a Kr laser focused on the sample to produce a spot of either a roundish shape of about 0.5 mm in diameter for the two-dimensional (dot cell) geometry or a 1 mm$\times$4 mm rectangular shape perpendicular to the linear cell for the 1D geometry.

Figure 4 shows that the measured V_{oc} in a completed (metallized) 1D cell gradually decays with the distance from the laser beam. In these experiments the laser-blocked V_{oc} $=517$ mV (corresponding to the ambient light intensity of the order of 10^{-4} sun) was far lower than the minimum signal measured under excitation. Hence, the perturbation decay length is considerably larger than the sample size. If we use the inverse logarithmic derivative as a quantitative measure of the screening length for the data in Fig. 4, then in all cases the latter turns out to be larger than 1 m, hence considerably exceeding the sample size. Following Eq. (9), the data were fit by

$$V_{oc}(x)=P_1-P_2\ln\left[\cos\left(\frac{\ell-x}{P_3}\right)\right], \tag{13}$$

where P_1, P_2, and P_3 are fitting parameters. From Fig. 4 we observe excellent agreement between the data and theoretical expression in Eq. (9). The best-fit parameter P_1 was found to depend on the excitation power logarithmically, which is consistent with Eqs. (9) and (10). The best-fit parameters P_2 in all cases were close to 80 meV, which, in accordance with Eq. (9), is double of the thermal energy (52 meV) multiplied by the nonideality factor. Finally, the best-fit parameters P_3 $=190$, 160, and 150 mm corresponding to the excitation powers of 6.8, 27.2, and 68 mW, respectively, are fully consistent with Eq. (10) if we make a reasonable assumption that the laser-generated current J_L is linear in the excitation power. A good agreement between the data and the theoretical prediction confirms our understanding of the phenomenon.

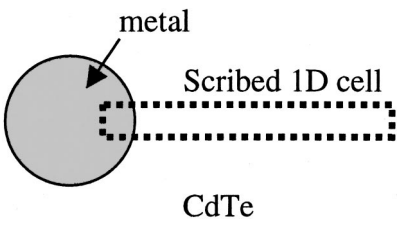

FIG. 3. Bottom view of a 1D cell scribed out of the 2D (dot) cell. The shaded area has a deposited metal contact. Scribes (dotted) penetrate to the TCO and thus insulate the designated strip from the rest of the substrate.

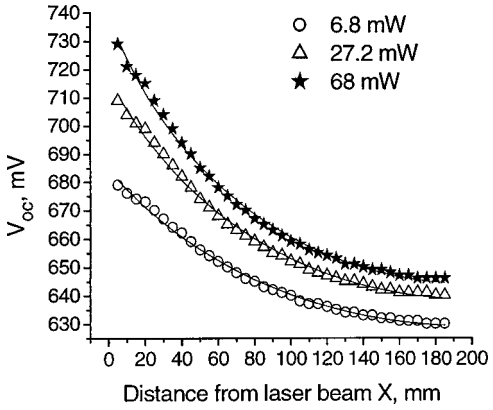

FIG. 4. Nonlocal V_{oc} vs the distance from the laser beam in 1D cell with the TCO-dominated lateral spreading for different excitation powers: data and theoretical fits.

Data for the semiconductor driven lateral spreading in 2D geometry (Fig. 5) also show smooth decay in V_{oc} with the characteristic screening length $\sim$1 mm, much shorter than that of the TCO-dominated spreading. Eq. (5) fits the data reasonably well as represented in the form

$$V_{oc}=P_1-P_2\ln\left(1+\frac{x}{P_3}\right). \tag{14}$$

One unfortunate feature was that the 3-parameter fit in Eq. (14) provides too much flexibility and thus leaves the parameters rather loosely defined. For example, from Fig. 5 and many other similar fits we were only able to estimate α $=0.3\pm0.2$.

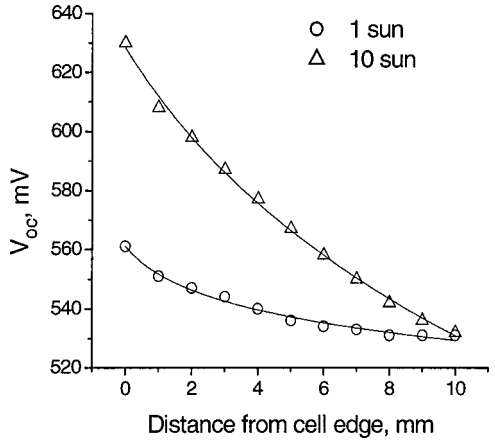

FIG. 5. V_{oc} vs distance from the 2D cell edge for semiconductor-dominated lateral spreading for two different laser power densities in comparison with theoretical fits: front-wall excitation.

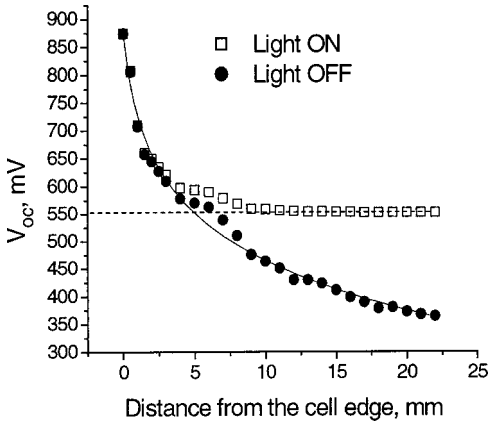

FIG. 7. V_{oc} vs distance from the laser beam for ambient light on and off. Vapor-transport deposited sample. Dashed line shows the saturated V_{oc} for the sample under ambient light.

In order to avoid the influence of metal contact on the measured V_{oc}, we conducted measurements with a nonmetal (carbon foam) small area contact as was described in the above in this section; some results typical of both VTD and magnetron sputtered sample are shown in Figs. 6 and 7. With the parameter P_2 set as 80 mV in Fig. 6 the data are best fit by the screening radii $P_3=1.9$ and 5.4 mm for the excitation power densities of 200 and 20 mW, respectively, which leads to a reasonable estimate $\alpha\sim 0.3$ in Eq. (7). The main observations are: (i) samples made by two different techniques show qualitatively the same behavior reasonably well fit by Eq. (5); (ii) the cases of ambient light on and off fit the same theoretical curve in the region where the signal exceeds the saturated V_{oc} by more than the thermal energy; (iii) the signal amplitudes do not depend on the ambient light. These observations agree with the theoretical predictions in Sec. II.

One other theoretical prediction is verified in Fig. 8, which shows similarity between the nonlocal responses from the 2D and 1D cell scribed out from the 2D cell in accordance with the design in Fig. 3. The noisier character of the 1D cell signal is most likely due to the material damage introduced by scribing. The mechanical and laser scribes were shown to generate the noise of comparable amplitudes.

In the front-wall geometry excitation experiments, care should be taken to rule out the possibility of inducing the nonlocal photovoltaic response by multiple light scattering in a 3-mm-thick glass substrate preceding the semiconductor layers. This was verified by measuring the nonlocal photovoltaic response in the back-wall geometry where the laser beam was incident on the CdTe (Fig. 9). The measured spatial dependence of the open-circuit voltage turns out to be qualitatively the same for the front-wall and back-wall geometries. The absolute value of the signal in the back-wall geometry is much lower because the light is strongly absorbed in the CdTe layer before junction and only a relatively small fraction of the electron-hole pairs survives.

As the laser-generated plasma spreads out, it can emit light from the areas beyond the beam spot. In particular, this may be evidenced in the difference between the same area PL maps measured at different excitation power densities, 2 suns and 20 suns Figs. 10(a) and 10(b). Note that the low intensity map shows the presence of the sample edge ($y=0$) at a distance of several millimeters, while it is not seen under the high intensity laser beam. We conclude that the

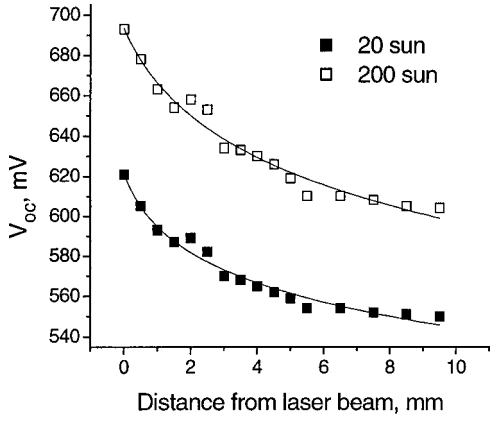

FIG. 6. V_{oc} vs distance from laser beam as measured with the nonmetal contact for two different excitation powers in comparison with the theoretical fits by Eq. (5).

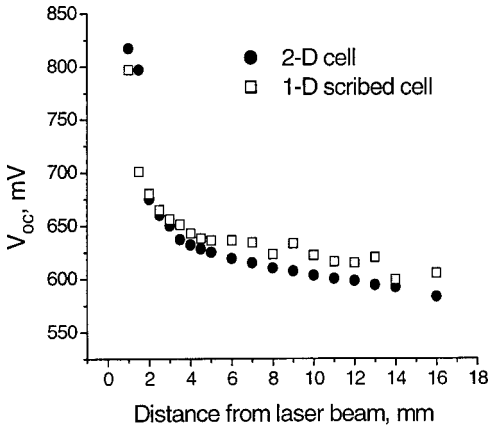

FIG. 8. V_{oc} spatial decay vs distance from the laser beam for a dot (2D) and a linear (1D) cell scribed from the 2D cell.

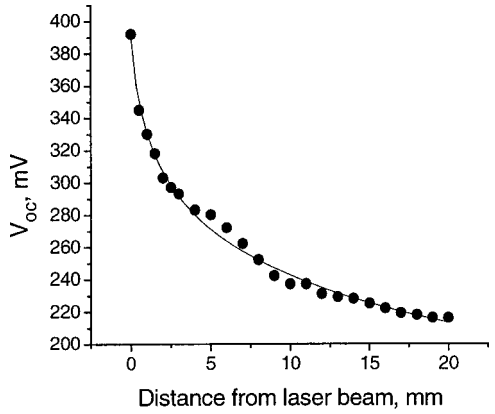

FIG. 9. Spatial decay of surface voltage in the case of back wall excitation. Laser power 25 mW.

plasma decay length decreases with increasing laser beam power as is predicted in Eq. (7) and verified by the V_{oc} measurements (cf. Fig. 6 and related earlier discussion).

We conclude this section by noting that, in general, our data show significant electron–hole plasma spreading even for the case of semiconductor-controlled lateral conductivity. The observed nonlocal photovoltaic response is consistent with the theoretical predictions in Sec. II. For the case of TCO-controlled spreading a good quantitative agreement between the theory and experiment is achieved. For the alternative case of semiconductor-controlled spreading the agreement is of semiquantitative nature. Noticeable dispersion in parameters determined for different nominally identical samples points at local in-plane resistivity fluctuations as possible source of uncertainty. In accordance with Eqs. (7) and (8), we can estimate from our data the semiconductor to TCO sheet resistance ratio as the square of the inverse ratio of the corresponding screening lengths. This gives the semiconductor sheet resistance of the order of 10^7–10^9 $\Omega/\square$, which is unexpectedly low as compared to the typical 10^{10}–10^{11} $\Omega/\square$ obtained by means of the four-point probe for the same material. The nature of this apparent inconsistency may again be attributed to the role of in-plane nonuniformity, which averages out over a considerable distance (correlation radius), exceeding L (see discussion in the end of Sec. II). More specifically, we can define the correlation radius as the distance between the most resistive elements in the array forming a nonuniform system.[13] Over shorter distances the system can then exhibit smaller than the average resistivity.

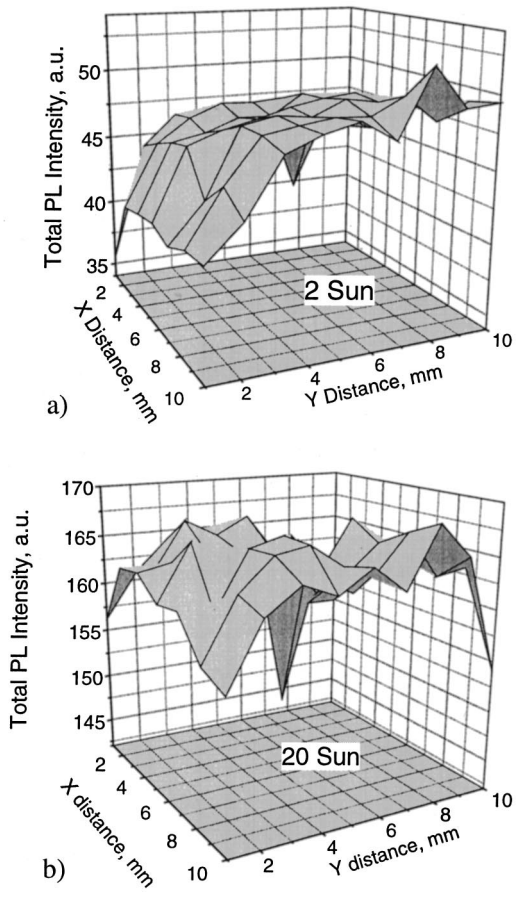

FIG. 10. PL maps corresponding to two different excitation power densities.

IV. CONCLUSIONS

In conclusion, we have observed nonlocal photovoltaic response to the laser beam excitation in CdTe photovoltaics. Our model relates these observations to spreading of the electron-hole plasma beyond the laser beam spot. We have introduced a concept of screening length that characterizes the distance over which the nonequilibrium electron–hole plasma decays. The screening length is shown to strongly depend on the device lateral resistance and excitation power, varying from more than 1 m for the TCO-controlled lateral spreading to tenths of a millimeter for the case of semiconductor-controlled spreading. Our theory provides a good quantitative agreement with the data for the former case and remains a reliable semiquantitative guide for the latter case where effects of nonuniformities bring more complexity to the phenomenon. One distinctive feature is that because of significant I/V characteristic nonlinearity, the spatial decay of the laser-generated voltage has a long-range nature and is logarithmic as opposed to the exponential decay in the standard transmission line.

One practical implication of the above results is that measuring the spatial decay of the open circuit voltage in a completed cell enables one to establish the dependence of the laser-generated current on the excitation power, which characterizes the device efficiency and recombination properties. The same measurements can be used to estimate the TCO sheet resistance in a completed device. For the case of semiconductor-controlled lateral spreading, practical implications can be related to the established unexpectedly low semiconductor layer sheet resistance. A consequence of this may be current loss caused by semi-shunts, which are metal protrusions partially penetrating the semiconductor film from one of the contacts. This will be discussed in more detail elsewhere. One other important practical conclusion pertains to the spatial resolution of the photoluminescence mapping, which, under open circuit conditions, was shown to strongly depend on the excitation power.

This work was partially supported by NREL Grant No. NDJ-1-30630-02.

APPENDIX

Introducing a new variable

$$u=\exp\left[-\alpha\frac{V_{oc}-\varphi}{T}\right], \tag{A1}$$

and noticing that, by definition,

$$\exp\left(\frac{V_{oc}}{T}\right)=\frac{j_L+j_0}{j_0}, \tag{A2}$$

Eqs. (1) and (4) can be reduced to

$$L_0^2\frac{d^2u}{dx^2}=u^{1/\alpha}-1. \tag{A3}$$

Multiplying the latter by du/dx and integrating gives

$$\frac{L_0^2}{2}\left(\frac{du}{dx}\right)^2=\frac{\alpha+1}{\alpha}u^{\alpha+1/\alpha}-u+\frac{1}{1+\alpha}, \tag{A4}$$

where the constant of integration is determined from the boundary condition at the infinity, $du/dx=0$ when $u=1$. For the case of strong perturbation, $u\gg 1$, only the first term in the right-hand side is kept. With that integrating Eq. (A4) yields

$$u=u_0\left(1\pm\frac{x}{L}\right)^{2\alpha/\alpha-1}, \quad L=L_0\sqrt{\frac{1+\alpha}{2\alpha}}u_0^{\alpha-1/2a}. \tag{A5}$$

The first of the boundary conditions Eq. (3) can be represented as

$$u_0=\frac{J_L L}{(j_L+j_0)L_0^2}\frac{1-\alpha}{2\alpha}. \tag{A6}$$

Solving Eqs. (A5) and (A6) leads to the final results in Eq. (5)–Eq. (8) in the main body of the text.

For the case of the finite size sample with TCO-dominated lateral effects we let $\alpha=0$ and integrate the equation

$$\frac{d^2z}{dy^2}=-\exp(-z), \tag{A7}$$

where $z=V_{oc}-\varphi/T$, $y=x/L_0$,
with the same boundary condition [Eq. (4)] at the beam edge and with the condition $dz/dy=0$ at the sample edge, $y=\ell/L_0$. This leads to results in Eqs. (9) and (10) in the main body of the text.

For the 2D case the second derivative is replaced by the Laplacian, and Eq. (A3) becomes

$$L_0^2\left(\frac{d^2u}{dx^2}+\frac{1}{x}\frac{du}{dx}\right)=u^{1/\alpha}-1. \tag{A8}$$

For the case of $x\gg L_0$, the second term in the left-hand side can be omitted, which reduces the problem to the 1D case, so that Eq. (A5) obeys. For the case of $x\ll L_0$, we note that any particular function $f(u,x)$ in

$$\frac{1}{x}\frac{\partial u}{\partial x}=f(u,x)$$

leads to

$$\frac{\partial^2u}{\partial x^2}=f(u,x)+x\frac{\partial}{\partial y}f(u,x).$$

Here the last term is relatively small as $y\ll L_0$ and $\partial f/f\partial y\sim 1/L_0$. Neglecting that term reduces Eq. (A8) to the form

$$L_0^2\frac{2}{x}\frac{du}{dx}=u^{1/\alpha}-1, \tag{A9}$$

which can be solved analytically to give

$$u=u_1\left[1\pm\left(\frac{x}{L}\right)^2\right]^{\alpha/\alpha-1}, \quad L=2u_1^{\alpha-1/2\alpha}L_0, \tag{A10}$$

with the parameter u_1 to be determined from the boundary condition Eq. (4) at $x=d/2$ with dJ/dx replaced by div **J**, and the sign choice determined by the boundary condition at infinity. From sewing at $x\sim L$ the expressions for $u(x)$ in Eqs. (A5) and (A10), it follows that $u_1\sim u_0$. As a result the screening lengths in Eqs. (A5) and (A10) coincide to within a numerical multiplier. A consequence of this is that the solution in the region $x\gg L$ can be approximated by applying the boundary condition at the beam edge directly to the expression $u(x)$ in Eq. (A5), which makes all the 1D results approximately applicable to the 2D case. One minor difference pertains to the region of small $x\ll L$, where the 2D solution for $\varphi(x)$ has negative curvature and a deflection point at $x\sim L$.

[1] N. Nango, S. Iida, and T. Ogawa, J. Appl. Phys. **86**, 6000 (1999).
[2] Z. F. Li, W. Lu, G. S. Huang, R. Yang, L. He, J. Appl. Phys. **90**, 260 (2001).
[3] S. A. Galloway, R. P. Edwards, and K. Durose, Inst. Phys. Conf. Ser. **157**, 579 (1997).
[4] R. Harju, V. G. Karpov, D. Grecu, and G. Dorer, J. Appl. Phys. **88**, 1794 (2000).
[5] J. F. Hiltner and J. R. Sites, in *Proceedings 28th IEEE Photovoltaic Specialists Conference*, Alaska, 2000, p. 543.
[6] S. A. Galloway, W. A. Brinkman, K. Durose, P. R. Wilshaw, and A. J. Holland, Appl. Phys. Lett. **68**, 3725 (1996).
[7] C. Christopolous, *The transmission Line Modeling Methods* (IEEE, New York, 1995).
[8] S. M. Sze, *Physics of Semiconductor Devices* (Wiley, New York, 1981).
[9] V. G. Karpov, G. Rich, A. V. Subashiev, and G. Dorer, J. Appl. Phys. **89**, 4975 (2001).
[10] A comment is in order regarding the case of polycrystalline semiconductors in which conductivity is dominated by the intergrain potential barriers. Because of the screening phenomenon, the intergrain barrier height depends on the carrier concentration, hence, on the local electric potential. This, in turn, leads to an exponential dependence $\rho(\varphi)$, which in the simplest approximation, can be accounted for by renormalizing the parameter α in Eq. (3). As a result, α is considered a phenomenological parameter, whose value can be either less or larger than unity or even negative.
[11] V. G. Karpov, R. Harju, and G. Dorer, in *Proceedings 28th IEEE Photovoltaic Specialists Conference*, Alaska, 2000, p. 547.
[12] R. H. Bube, *Photovoltaic Materials* (Imperial College Press, London, 1998).
[13] A. L. Efros and B. I. Shklovskii, *Electronic Properties of Doped Semiconductors* (Springer, Berlin, 1992).